

# Diffraction polychromator for Raman lidar

S.N. Volkov, M.M. Makogon, and V.I. Serdyukov

*Institute of Atmospheric Optics,  
Siberian Branch of the Russian Academy of Sciences, Tomsk*

Received October 5, 2004

An original optical layout of a polychromator for Raman lidar is proposed, whose advantages are the ease of fabrication and efficiency in use. A method for calculation of a two-step diffraction polychromator is presented. The polychromator design, adjustment methods, and test results are described.

## Introduction

In Raman lidars, backscattered signals result from the laser excitation of rotational and ro-vibrational transitions in molecules and the resultant re-emission at shifted wavelengths. Since the spontaneous Raman light scattering is almost instantaneous process,<sup>1</sup> the spatial resolution of the obtained data is equal to the exciting laser pulse length. Due to the facts that manifestation of the stimulated Raman scattering is independent of the exciting radiation wavelength, and molecules can be identified by their spectra, as well as the intensity of SRS lines is directly proportional to the gas concentration, this method is promising in sensing trace gases, as well as gaseous pollutant emissions from industrial objects, power stations, and traffic.

The main advantage of the Raman lidar method is a possibility of detecting and measuring the content of many atmospheric trace gases with the use of a single laser, operating at a fixed wavelength.

For the first time, the Raman scattering was used in determination of atmospheric molecules (nitrogen and oxygen) by Leonard in 1967 (Ref. 2). Since then a great quantity of Raman lidars have been developed.<sup>3,4</sup> These systems are capable of measuring both minor atmospheric pollutions and local emissions into air basins of industrial centers. The Raman lidar was used for remote monitoring of fuel gas flows from smoke stacks of heat and power plants.<sup>5</sup> Remote Raman systems measured the atmospheric temperature by the rotational Raman spectroscopy method.<sup>6,7</sup>

The method's appeal is in its ability to determine the gas absolute concentration by comparing its SRS signals to SRS signals from molecular nitrogen, which are used as a standard in the atmospheric sensing; in addition, it can be metrologically tested unlike other laser sensing methods.

By now, the concentrations of such trace gases as CO, CO<sub>2</sub>, SO<sub>2</sub>, C<sub>2</sub>H<sub>4</sub>, H<sub>2</sub>CO, NO, H<sub>2</sub>S, C<sub>3</sub>H<sub>4</sub>, as well as such compounds as cyclohexane, isopropyl, acetone, and others in the surface atmosphere have been measured with the use of Raman lidars.<sup>1,8,9</sup> In addition, NASA reported the application of a DC-8 Raman lidar for remote measurements of methane, water vapor, and temperature aboard a flying laboratory. However, modern Raman lidars have found a wide utility only

in sensing of water vapor and temperature in the troposphere.<sup>10–12</sup>

A certain disadvantage of the Raman sensing method is small Raman scattering cross sections of atmospheric constituents (two to three orders of magnitude smaller than those for Rayleigh scattering and many orders of magnitude smaller than for aerosol scattering). Therefore, the needed signal-to-noise ratio in the lidar can be achieved due to increased requirements to the energy and spectral characteristics: high energy and peak power of laser pulses, as well as to the spectral instrumentation.

Evidently, the limited use of Raman lidars in measurements of gaseous pollutants is because of their main disadvantage: weak return signals (due to weak interaction and low concentration of gaseous constituents under testing), which are difficult to distinguish against the background of elastic scattering signals, as well as possible overlapping of Raman spectra of different molecules (mixing of signals). The solution of these problems requires the spectral selection and sensitivity of the receiving system to be improved significantly. In this paper, we describe a newly developed version of a high-selectivity spectral device for general-purpose Raman lidars.

The requirements imposed on polychromators for Raman lidars are listed below:

- 1) simultaneous separation of several (as a rule, about 10) analytical spectral ranges: from 5 to 8 Raman lines of analyzed gases and Raman lines of nitrogen and oxygen;
- 2) the spectral width of the pass band in each channel no more than 6–8 cm<sup>-1</sup> (the width of the Q-branch of a ro-vibrational band);
- 3) no less than 12–13 orders of magnitude suppression by the polychromator of the scattered radiation at the unbiased frequency;
- 4) as high as possible transmittance of the spectral device;
- 5) the connection of the polychromator with the receiving telescope and photodetector through optical waveguides is desirable.

The first requirement actually determines the structure of the device, because only spectral device of high angular dispersion can distribute radiation in a large number of spectral channels. In the visible

spectral region, a diffraction grating is much more efficient than a prism, therefore, it is worth designing the spectral selector on the basis of a diffraction spectrometer. The needed suppression of the scattered radiation at an unbiased frequency can be achieved through using the second stage of the diffraction polychromator or additional filters.

## Design of the polychromator

For many decades, the assortment of optical elements for designing spectral devices is the same: mirror, lens, prism, and diffraction grating. Application of new technologies in manufacturing optical elements allows to gradually extend their qualitative range: to create new optical materials with ultrahigh refractive index, holographic diffraction gratings and holographic filters, to use optical waveguides for connection of optical elements.

As always, the decisive factor in the use of novel technologies in optical devices is optimal relation between the quality and the price. Therefore, particularly valuable are constructive solutions simplifying the design. For example, the use of waveguides as optical couplers in lidars has provided for mechanical stability of parameters and allowed us to locate the optical elements, sensitive to the atmospheric or electrical acting, under more favorable conditions.

The most difficult problem proved to be a decrease of losses in spectral devices of Raman lidars. The Fastie–Ebert monochromator scheme is widely used, because it favors decreasing aberrations in the dispersion plane. This allows the needed spectral resolution to be achieved in a rather simple way at slight optical distortions. However, aberrations in the perpendicular plane increase then significantly, that leads to energy losses. Therefore, the application of such an optical scheme assumes powerful radiation sources and long time intervals for recording the spectrum. Consequently, their use in Raman lidars, sensitive to radiation losses, becomes problematic.

A traditional technological solution, namely, a transition into the autocollimation mode, only slightly decreases the energy losses. In this connection, to be noted is the mirror scheme of the Pfund monochromator<sup>14</sup> and lens optical objectives. A characteristic feature of such solutions is the use of difficult-to-make parabolic mirrors or multicomponent optical objectives, which significantly raise the price of the Raman lidar and restrict the domain of its applicability mostly to large scientific research centers.

We propose an original optical scheme of a polychromator based on the modified Fastie–Ebert scheme, operating in the autocollimation mode and free of these disadvantages (Fig. 1). A key moment is the use of a holographic grating and waveguides as entrance and exit slits of the polychromator, as well as the arrangement of optical elements, which allows the standard spherical mirror to be used at a polychromator aperture of 1:5.

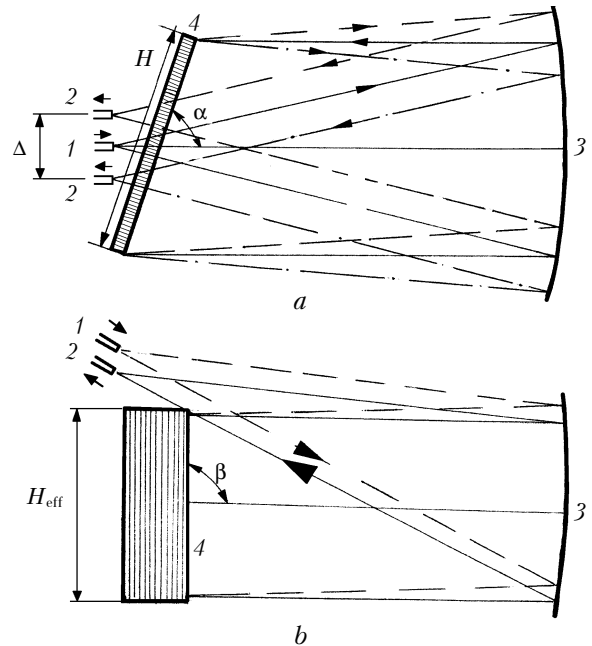


Fig. 1. Selector of the Raman lidar: view in the dispersion plane (a), view in the perpendicular plane (b); input waveguide 1; output waveguides 2, mirror 3, diffraction grating 4.

The device operates in a rather narrow spectral interval and does not require tuning in the process of operation. By choosing the angle  $\alpha$ , the grating is set so that it can operate in the autocollimation mode at the average wavelength  $\lambda_{av}$ . The angle  $\beta$  is chosen so that the plane of output waveguides is separated from the input waveguide by the distance no longer than it is needed for their fixation (1–2 mm); the waveguides are also set as close as possible to the grating.

The polychromator parameters satisfy the following relations:

$$\lambda_{av} = (\lambda_{min} + \lambda_{max})/2; \quad (1)$$

$$\varphi = \arcsin(K\lambda_{av}/2t); \quad (2)$$

$$H_{eff} = H\cos\varphi; \quad (3)$$

$$\Delta l = (\lambda_{i+1} - \lambda_i)D_1, \quad (4)$$

$$\Delta = (\lambda_{max} - \lambda_{min})D_1, \quad (5)$$

$$\Delta v_c = d_{wg}/(\lambda^2 D_1); \quad (6)$$

$$D_1 = 2F\varphi/\lambda; \quad (7)$$

$$F = H_{eff}/0.25, \quad (8)$$

where  $\varphi$  is the angle of radiation incidence onto the grating;  $K$  is the diffraction order;  $t$  is the grating constant;  $H_{eff}$  is the size of the grating projection onto the direction of the incident radiation;  $\Delta l$  is the distance between waveguides, into which the radiation of spectrally neighboring Raman bands of detected gases is outputted;  $\Delta$  is the maximal distance between waveguides;  $D_1$  is the linear dispersion of polychromator;  $\Delta v_c$  is the polychromator pass band;

$d_{wg}$  is the waveguide diameter;  $F$  is the focal length of the polychromator collimator.

Since the angular aperture of the waveguide is  $1/4$ , the focal length of the collimator and the grating size are related by the last equation.

Table 1 presents calculated parameters of a grating-based spectral selector. The grating has 600 lines/mm and operates in the 3rd, 4th, and 5th orders. The waveguide diameter was assumed equal to 1 mm. For definiteness, major gaseous atmospheric pollutants were considered. It follows from Table 1 that any considered grating can provide for the needed pass band, but as the diffraction order decreases, the grating size should be increased. At the same time, with the diffraction order increase, the ratio  $\Delta/F$  increases, that leads to a higher aberration of beams and some decrease of the diffracted radiation, collected by the output waveguides. A 150 mm wide grating, having 600 lines/mm and operating in the 4th order, can be used as a spectral device. The same characteristics can be achieved with gratings having 1200 and 2400 lines/mm, operating in the 2nd and the 1st diffraction orders, respectively. The grating must be chosen based on the analysis of the efficiency of radiation diffraction into the working order, the quality, and the price.

The second polychromator can follow the same scheme (Fig. 2), and it must provide for the autocollimation mode at any wavelength. The distance between the extreme waveguides  $\Delta_1$  is shorter than  $\Delta$  in the first stage, and for the 150-mm grating with 600 lines/mm, operating in the 4th order, it is 43.08 mm. The second polychromator has the same selectivity as the first one. The additional advantage of using the double polychromator is the improved suppression of radiation not only at the laser wavelength, but also of neighboring Raman bands, which is especially important when detecting, for example, small amounts of  $\text{NO}_2$  against a background of a high concentration of  $\text{CO}_2$ .

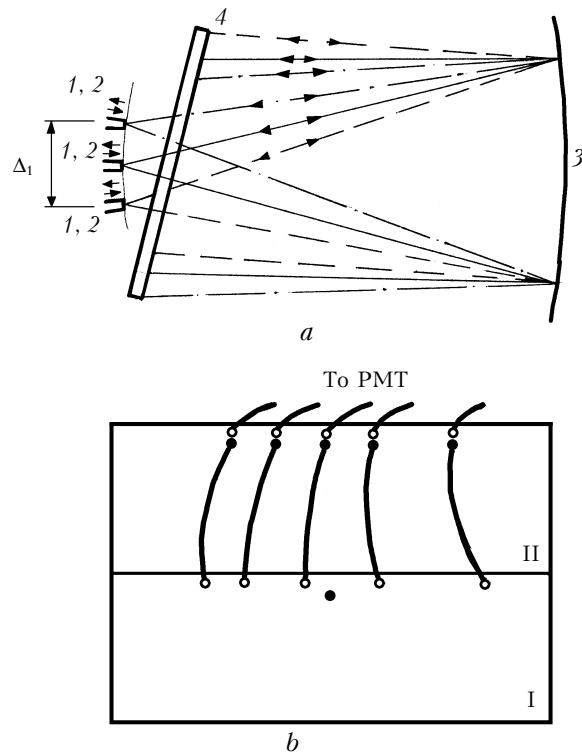


**Fig. 2.** Scheme of the second polychromator (a) and view of the double spectrally selective device from the side of waveguides (b): I and II are the first and the second stages of the polychromator; input waveguides are shown by closed circles, and output ones are shown by open circles; input waveguides 1, output waveguides 2, mirror 3, diffraction grating 4.

### Calculation of aberrations

The standard aberration analysis of the polychromator designed by the Fastie–Ebert scheme is suitable, to a greater extent, for visual control of the image quality. The control of energy image spread

**Table 1.** Main design parameters of polychromators

$K$	3			4						5		
	$\Delta l$ , mm	$\Delta l/d_{wg}$	$\Delta v_c$	$\Delta l$ , mm	$\Delta l/d_{wg}$	$\Delta v_c$	$\Delta l$ , mm	$\Delta l/d_{wg}$	$\Delta v_c$	$\Delta l$ , mm	$\Delta l/d_{wg}$	$\Delta v_c$
$\varphi$ , deg	32.43			45.64						63.35		
$H$ , mm	200			150		120				120		
$H_{eff}$ , mm	168.81			104.87		83.89				53.82		
$F$ , mm	675.24			419.47		335.57				215.30		
$KH/t$	360000			360000		288000				360000		
Gases	$\Delta l$ , mm	$\Delta l/d_{wg}$	$\Delta v_c$	$\Delta l$ , mm	$\Delta l/d_{wg}$	$\Delta v_c$	$\Delta l$ , mm	$\Delta l/d_{wg}$	$\Delta v_c$	$\Delta l$ , mm	$\Delta l/d_{wg}$	$\Delta v_c$
$\text{SO}_2$	7.893	26.312	6.169	7.893	26.312	6.169	6.315	21.049	7.711	7.893	26.312	6.169
$\text{NO}_2$	3.219	10.731	6.110	3.219	10.731	6.110	2.575	8.585	7.637	3.219	10.731	6.110
$\text{CO}_2$	8.062	26.875	6.086	8.062	26.875	6.086	6.450	21.500	7.608	8.062	26.875	6.086
$\text{O}_2$	15.850	52.835	6.027	15.850	52.835	6.027	12.680	42.268	7.534	15.850	52.835	6.027
$\text{NO}$	13.701	45.672	5.915	13.701	45.672	5.915	10.961	36.537	7.394	13.701	45.672	5.915
$\text{CO}$	9.771	32.572	5.821	9.771	32.572	5.821	7.817	26.057	7.277	9.771	32.572	5.821
$\text{N}_2$	27.396	91.321	5.756	27.396	91.321	5.756	21.917	73.057	7.195	27.396	91.321	5.756
$\Delta$ , mm	85.895			85.895		68.716				85.895		
$\Delta/F$	0.12720			0.20477		0.20477				0.39895		

parameters is more efficient with the approach based on the analysis of the image of a point object or object of a finite size. At such a consideration, the radiation sources with spatial and angular characteristics, imitating, for example, the input waveguide, are located in the object plane. The computational algorithm is constructed as follows: the object is divided into a series of point sources, whose radiation propagates through the optical system having aberrations, and the image of the source as a whole is formed in the image plane with allowance for the energy weight of each point source. Thus, based on the photometric analysis of the image, it is possible to determine a suitable size of the output waveguide consistent with the input one. In addition, taking into account the inhomogeneity of the image spread, it is possible to determine the corrected coordinates of waveguides providing for the maximal energy transfer. Such photometric analysis is most suitable for estimation of characteristics of polychromators, constructed with the use of waveguides.

The radiation propagation from a point source can be calculated in different approximations, in particular, in the ray approximation (here rays mean the normals to wave fronts). The ray approximation is based on solution of the Helmholtz equation

$$\nabla^2 u(x, y, z) + k^2 u(x, y, z) = 0, \quad (9)$$

where  $k = 2\pi/\lambda$  is the wave vector. In such a way, we perform a transition to the ray propagation, corresponding to the Fermat principle.

The solution of the wave equation can be obtained in the form of spherical or plane waves. For the Gaussian beams propagating in the direction  $z$ , corresponding to the radiation outgoing from the waveguide, the solution can be represented as

$$u(x, y, z) = \psi\{x, y, z\} \exp(\pm ikz), \quad (10)$$

where  $\psi\{x, y, z\}$  is the amplitude-phase function, being the solution of the wave equation

$$\frac{d^2\Psi}{dx^2} + \frac{d^2\Psi}{dy^2} + \frac{d^2\Psi}{dz^2} - 2ik \frac{d\Psi}{dz} = 0. \quad (11)$$

Since the beam propagates along the axis  $z$ ,  $\psi\{x, y, z\}$  should satisfy so-called paraxial (or parabolic) wave equation

$$\frac{d^2\Psi}{dx^2} + \frac{d^2\Psi}{dy^2} - 2ik \frac{d\Psi}{dz} = 0. \quad (12)$$

Its solution, found through the orthogonal functions, looks like

$$u(x, y, z) = \frac{w_0}{w(z)} H_m\left(\frac{\sqrt{2}}{w}x\right) H_n\left(\frac{\sqrt{2}}{w}y\right) \times \exp\left[-i(kz - \Phi(z)) - r^2\left(\frac{1}{w^2(z)} + \frac{ik}{2R(z)}\right)\right], \quad (13)$$

$$r^2 = x^2 + y^2, \quad \Phi(z) = \arctan[\lambda z / (\pi w_0^2)]. \quad (14)$$

Functions  $H_m$  and  $H_n$  are Hermitian polynomials:

$$H_0(\xi) = 1,$$

$$H_1(\xi) = 2\xi,$$

$$H_n(\xi) = (-1)^n e^{\xi^2} \frac{d^n}{d\xi^n} e^{-\xi^2}, \quad (15)$$

and  $w(z)$  and  $R(z)$  are the width and the curvature radius of the Gaussian beam;  $w_0$  is a constant.

Representing the radiation source by a set of rays with the probability density  $p(x)$  and  $p(y)$ , we pass on to the statistical description of the image spread. The second central moment, determining the image size, is

$$\sigma^2 = \int_{-\infty}^{\infty} (x - \langle x \rangle)^2 p(x) dx. \quad (16)$$

For  $n$  rays with the weights  $w_i$ , traversed through the optical system, in the displacement coordinates  $\{\Delta X$  and  $\Delta Y\}$  in the image plane with respect to the axis of the central (apical) ray, the second moments are

$$\sigma_x^2 = \frac{1}{W} \sum_{i=1}^n w_i (\Delta X_i - \langle x \rangle)^2, \quad (17)$$

$$\sigma_y^2 = \frac{1}{W} \sum_{i=1}^n w_i (\Delta Y_i - \langle y \rangle)^2,$$

where

$$W = \sum_{i=1}^n w_i. \quad (18)$$

Extracting the roots from the second central moments, we obtain the root-mean-square (RMS) values of the image spread.

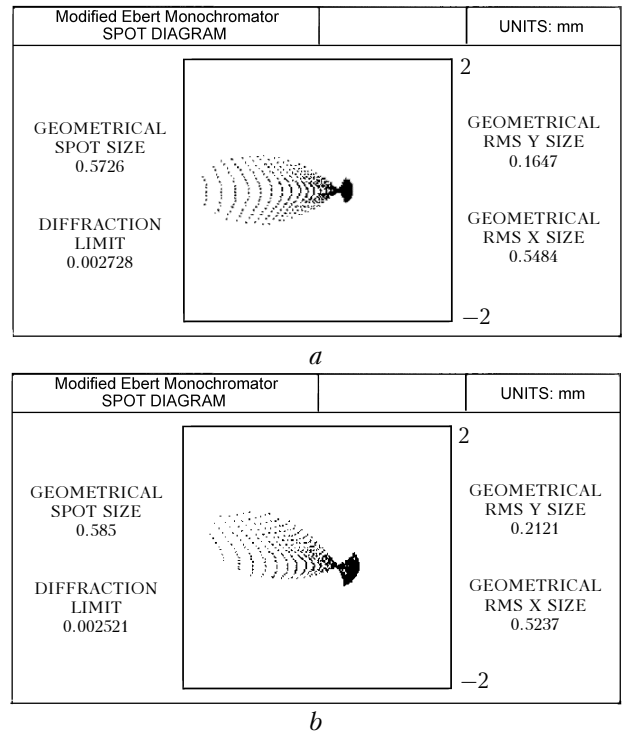


Fig. 3. Spot from a point source at the center (a) and the edge (b) of the image field.

A program package was developed to perform the calculations and display the results. The calculations were carried for the polychromator, intended for the use in the Raman lidar with a copper vapor laser (wavelength of 0.51055  $\mu\text{m}$ ) as a source of radiation. The results of calculation are shown in Fig. 3. As can be seen, the radiation spot in the plane of the waveguide output end is not circular, therefore, the fraction of radiation entering the waveguide (collection coefficient) depends on the output waveguide diameter (Table 2).

**Table 2. Coefficients of collection  $K_{\text{col}}$  of the nitrogen Raman radiation (input waveguide diameter of 0.8 mm,  $\lambda = 0.57952 \mu\text{m}$ )**

Shift in the image plane, mm	Output waveguide diameter, mm	$K_{\text{col}}$ , %
0	1.0	92.7
0	1.2	98.0
4.5543	1.0	77.5
4.5543	1.2	88.3

In addition, for more efficient collection of radiation, the waveguide should be somewhat shifted with respect to the position, calculated with neglect of aberrations (Table 3).

**Table 3. Calculated coordinates for output of Raman scattering, mm**

Gas	$\Delta\nu$ , $\text{cm}^{-1}$	$\lambda$ , $\mu\text{m}$	$X$	$X_{\text{cor}}$	$Y$	$Y_{\text{cor}}$	
SO <sub>2</sub>	1151	0.54243	-6.9779	-7.0179	35.2892	35.3274	
NO <sub>2</sub>	1320	0.54744	-6.2859	-6.3259	25.9869	26.015	
CO <sub>2</sub>	1388	0.54949	-5.9978	-6.0378	22.1452	22.1691	
O <sub>2</sub>	1556	0.55461	-5.2654	-5.3054	12.457	12.4705	
NO	1877	0.56466	-3.771	-3.811	-6.97307	-6.9806	
CO	2145	0.57334	-2.4146	-2.4546	-24.2366	-24.2628	
N <sub>2</sub>	2331	0.57952	-1.4082	-2.4482	-36.8285	-36.8683	
Hg	1	-	0.546074	-6.4762	-6.5162	28.5352	28.566
	2	-	0.567586	-3.3209	-3.3609	-12.7401	-12.7539
	3	-	0.57696	-1.8293	-1.8693	-31.5806	-31.6147
	4	-	0.579016	-1.4916	-1.5316	-35.7917	-35.8304
	5	-	0.580365	-1.2678	-1.3078	-38.571	-38.6127

The obtained data suggest that a proper selection of the waveguide can provide for no lower than 90% photometric efficiency of the polychromator.

## Polychromator construction

In our design, we use waveguides to input radiation into the polychromator and to output the diffracted radiation. Waveguide ends are confined in metal clips, which are fixed in a figured plate (mask), set so that the waveguide ends are in the image plane. The positions of holes for waveguide fixation are determined by the wavelengths the polychromator is tuned to. In our case, it is tuned to detection of atmospheric nitrogen and oxygen, nitrogen and carbon oxides, as well as nitrogen, carbon, and sulfur dioxides. The plate also has 5 holes for fixation of waveguides, intended for radiation of 5 emission lines of a mercury lamp, which is used for tuning the polychromator.

The shift  $L$  of the input waveguide image with respect to the axis, corresponding to its image at the blaze angle, is determined by the equation

$$L = F \tan [\phi(\varphi, k, \Delta\nu) - \phi(\varphi, k, 0)], \quad (19)$$

where

$$\phi(\varphi, k, \Delta\nu) = \arcsin \left( \frac{k}{t(v_0 - \Delta\nu)} - \sin\varphi \right), \quad (20)$$

$\phi$  is the diffraction angle;  $\Delta\nu$  is the Stokes frequency shift;  $v_0$  is the frequency of the exciting laser radiation. The results of calculation of the shifts by Eq. (19) are presented in Table 3 (columns  $X$  and  $Y$ ; the coordinate  $X$  corresponds to the position of the output waveguides with respect to the input one in the plane perpendicular to dispersion, the coordinate  $Y$  is the same in the dispersion plane). The columns  $X_{\text{cor}}$  and  $Y_{\text{cor}}$  present the shift values corrected with allowance for the aberration distortion of the image.

As a part of the lidar instrumentation, the polychromator may operate under rather severe conditions, including, first of all, vibrations and significant temperature differences (up to 60°C). Therefore, its design must be sufficiently rigid, but simple and allowing adjustment, which forms the basis for operation of the lidar system as a whole.

We have calculated the loads, arising in the polychromator due to the weight of the mirror and the diffraction grating in mounts. We calculated both the deformation of the carrier elements and temperature distortions. As a result of the analysis, we have accepted the polychromator design, in which all components are fixed on a rigid framework formed by four invar rods and two metal plates. One plate carries the mirror in the mount, fixed by adjusters, while another plate carries the diffraction grating in the mount and an alignment table, housing the waveguide unit (mask with waveguides).

The polychromator framework is placed inside a light-protecting jacket, ensuring also the light opacity of the input waveguide unit. The jacket is equipped with a light-opaque cap, providing for the convenient access to the adjusting table with waveguides. The external appearance of the polychromator is shown in Fig. 4.

The polychromator was adjusted and tested with the test radiation of Hg gas-discharge lines. The same technique, as was used to calculate positions of Raman lines of gases, was applied to calculate the line positions in the range 0.54–0.58  $\mu\text{m}$  (see Table 3). In accordance with these calculations, holes arranged in two lines were made in the receiving mask. The first line was for the waveguides, receiving the radiation of Raman lines and one Hg line ( $\lambda = 0.579016 \mu\text{m}$ ), while the second line was for the input waveguide of the polychromator and the waveguides, receiving the radiation of other Hg lines.

The adjustment of the receiving mask to the test radiation (second line) automatically led to full adjustment of the first line after the vertical shift of the mask and its alignment by only one Hg line ( $\lambda = 0.579016 \mu\text{m}$ ).



Fig. 4. External appearance of the polychromator.

The experiment has shown that the mask shift back into the second line changes the Hg line signal by no more than 1–5%, which corresponds to the mask misalignment by no more than 0.02 mm.

We used in the polychromator construction the hologram diffraction grating with 2400 lines/mm, operating in the first order (fabricated at the State Institute of Applied Optics). The scattering in this grating is at least two orders of magnitude lower than in ruled gratings (replica gratings). Note that the need of using the second polychromator in a lidar for suppression of sensing radiation scattered by aerosol should be determined as applied to particular measurement conditions. Along with the second polychromator, the suppression of radiation scattered at the laser radiation wavelength can be achieved by using:

1) spectrally selective interference coatings on the mirrors of the scanning system and the telescope;

2) bandstop filter (Notch-filter) before the radiation input into the spectral selector (for example, filters fabricated by Kaiser Optical Systems, Inc.<sup>13</sup> at the rejected wavelength have the optical density higher than 6 at a transmittance no lower than 75% in the working range);

3) proper bandpass filters (colored glasses);

4) additional narrowband interference filters intended for particular Raman wavelength and installed in front of the corresponding photodetectors.

## References

1. E.D. Hinkley, ed., *Laser Monitoring of the Atmosphere* (Springer Verlag, New York, 1976).
2. O.K. Kostko, V.S. Portasov, V.U. Khattatov, and E.A. Chayanova, *Application of Lasers to Determination of the Atmospheric Composition* (Gidrometeoizdat, Leningrad, 1983), 216 pp.
3. R.M. Measures, *Laser Remote Sensing* (Wiley, New York, 1987).
4. V.M. Zakharov, ed., *Laser Sensing of the Atmosphere from Space* (Gidrometeoizdat, Leningrad, 1988), 216 pp.
5. Yu.F. Arshinov, S.M. Bobrovnikov, V.K. Shumskii, A.G. Popov, and I.B. Serikov, *Atmos. Oceanic Opt.* **5**, No. 5, 323–328 (1992).
6. A. Cohen, J. Cooney, and K. Geller, *Appl. Opt.* **15**, No. 11, 2896–2901 (1976).
7. Yu.F. Arshinov, S.M. Bobrovnikov, V.E. Zuev, and V.M. Litov, in: *Spectroscopic Methods of Atmospheric Sensing* (Nauka, Novosibirsk, 1985), pp. 94–107.
8. V.M. Zakharov, O.K. Kostko, and S.S. Khmelevtsov, *Lidars and Investigations of Climate* (Gidrometeoizdat, Leningrad, 1990), 320 pp.
9. M.D. Ray and Ar.J. Sedlacek, in: *19th ILRC* (NASA, USA, 1998), pp. 677–679.
10. *Third International Lidar Researchers Directory*, compiled by M.P. McCormick (NASA, USA, 1993), 180 pp.
11. *Abstracts of the 19th International Laser Radar Conference* (NASA, USA, 1998), 986 pp.
12. *Advances in Laser Remote Sensing: Selected Papers of the 20th ILRC* (Vichy, France, 2000), 492 pp.
13. www.kosi.com.
14. K.I. Tarasov, *Spectral Devices* (Mashinostroenie, Leningrad, 1977), 360 pp.